Remote Sensing of Environment 232 (2019) 111349

Contents lists available at ScienceDirect

Remote Sensing of Environment

journal homepage: www.elsevier.com/locate/rse

A semi-analytical approach for remote sensing of trophic state in inland waters: Bio-optical mechanism and application

Kun Shi[a,b,c,*], Yunlin Zhang[a,b], Kaishan Song[d], Mingliang Liu[e], Yongqiang Zhou[a,b], Yibo Zhang[a,b], Yuan Li[a,b], Guangwei Zhu[a,b], Boqiang Qin[a,b]

[a] Taihu Laboratory for Lake Ecosystem Research, State Key Laboratory of Lake Science and Environment, Nanjing Institute of Geography and Limnology, Chinese Academy of Sciences, Nanjing 210008, China
[b] University of Chinese Academy of Sciences, Beijing 100049, China
[c] CAS Center for Excellence in Tibetan Plateau Earth Sciences, Beijing 100101, China
[d] Northeast Institute of Geography and Agricultural Ecology, Chinese Academy of Sciences, Changchun 130102, China
[e] Hangzhou Institute of Environment Science, Hangzhou 310014, China

ARTICLE INFO

Edited by Menghua Wang

Keywords:
Trophic status
Landsat 8 OLI
Absorption coefficients
Quasi-analytical algorithm (QAA)
Optically active constituents

ABSTRACT

The trophic state index (TSI) is a vital parameter for aquatic ecosystem assessment. Thus, information on the spatial and temporal distribution of TSI is critical for supporting scientifically sound water resource management decisions. We proposed a semi-analytical approach to remotely estimate TSI based on Landsat 8 OLI data for inland waters. The approach has two major steps: deriving the total absorption coefficient of optically active constituents (OACs) and building the relationship between the total absorption coefficient and TSI. First, version 6.0 of the Quasi-Analytical Algorithm (QAA_V6, developed by Zhongping Lee) was implemented with Landsat 8 OLI data to derive the total absorption coefficients of the OACs. Second, we modeled TSI using the total absorption coefficients of OACs at 440 nm based on a large in situ measurement dataset. The total absorption coefficient of OACs at 440 nm gave satisfactory validation results for modeling TSI with a mean absolute percent error of 6% and a root-mean-square error of 5.77. Then, we performed this approach in three inland waters with various eutrophic statuses to validate its results, and the approach demonstrated a robust and satisfactory performance. Finally, an application of the approach was demonstrated in Lake Qiandaohu. Our semi-analytical approach has a sound optical mechanism and extensive application for different trophic inland waters.

1. Introduction

Under the background of global climate change, ecosystem response, feedback, simulation, forecasting and assessment are currently hot topics of ecology and global change (Piao et al., 2008; Soliveres et al., 2016; Temmerman et al., 2013). Climate change has produced various lasting impacts on aquatic systems (Pekel et al., 2016). To assess and predict the global impacts of climate change, we need to understand natural variations in aquatic systems, such as the trophic states of inland waters around the world. Trophic state is the foundation of aquatic ecosystem assessment and is inextricably related to the biotic integrity and water quality of inland waters because it describes the energy available to the food web (Dodds, 2007). The trophic state index (TSI) has been built most extensively for inland waters, in large part as a result of relations to water quality issues. In inland waters, TSI is functionally determined by these parameters linked to autotrophic production, including phytoplankton biomass, levels of nutrients in the water column, and water clarity (Carlson, 1977; Pace et al., 2017; Walsh et al., 2016).

Thus, TSI is commonly adopted by the general ecological community, as well as limnologists and lake managers, for guiding and managing the ecosystems and water quality of inland waters. Characterizing TSI in inland waters is therefore vital for understanding lake ecosystems structure and functioning, as well as for understanding the biogeochemical features of lakes and conducting subsequent water quality and ecosystem health assessments (Kaunzinger and Morin, 1998; Thackeray et al., 2016). Thus, there is an especially urgent and critical need for highly spatially and temporally extensive information on the TSI of global inland waters to understand the variations in aquatic systems under climate change and to support scientifically

* Corresponding author at: Taihu Laboratory for Lake Ecosystem Research, State Key Laboratory of Lake Science and Environment, Nanjing Institute of Geography and Limnology, Chinese Academy of Sciences, Nanjing 210008, China.
E-mail address: kshi@niglas.ac.cn (K. Shi).

https://doi.org/10.1016/j.rse.2019.111349
Received 5 September 2018; Received in revised form 23 July 2019; Accepted 25 July 2019
0034-4257/ © 2019 Elsevier Inc. All rights reserved.

sound water resource management decisions. Nevertheless, it is difficult to use traditional field-lab methods to provide such scientific knowledge on the TSI of global inland waters.

Traditionally, the TSI of inland waters is mostly determined by four or more water quality parameters, namely, chlorophyll *a* (Chl*a*), total nitrogen (TN), total phosphorus (TP), and Secchi disk depth (SDD). Chl*a*, TN, and TP are measured using chemical approaches in the laboratory (Wetzel and Likens, 2010). Several labor- and time-consuming processes, such as field water sample collection, transportation, sample filtration, and chemical analysis, are necessary to measure these three chemical parameters (Dodds, 2007). This undoubtedly greatly inhibits the rapid assessment and characterization of TSI in inland waters undergoing a rapidly changing environment. In addition, the traditional approach is ill suited for monitoring a large number of inland waters at regional, national and global scales due to the patchy distributions of nutrients, Chl*a*, and SDD with the limited temporal and spatial scales (Sass et al., 2007).

For over 40 years, satellite remote sensing has been implemented to monitor several water trophic indexes of lakes, such as Chl*a* (Dall'Olmo et al., 2003; Gons et al., 2008; Gower et al., 2005; Hunter et al., 2008; Kutser, 2004; Matthews et al., 2012; Ryan et al., 2009), SDD (Binding et al., 2007; Olmanson et al., 2008), and nutrients (TN and TP) (Kutser et al., 1995; Song et al., 2012). Chl*a* is usually considered an indicator of phytoplankton and thus is a critical index of the water trophic state (Carlson, 1977; Mouw et al., 2015). A series of algorithms, such as Fluorescence Line Height (FLH) (Ryan et al., 2009), MERIS Maximum Chlorophyll Index (MCI) (Gower et al., 2005), Synthetic Chlorophyll Index (SCI) (Shen et al., 2010), Peak-Height Algorithm (MPH) (Matthews et al., 2012), band ratio (Red/NIR bands) method (Hunter et al., 2008), and three-band method (Dall'Olmo et al., 2003), has been developed to derive Chl*a* information from remote sensing data. However, the optimal band positions and parameters of the Chl*a* retrieval algorithms mentioned above generally vary with different water bodies. SDD is a basic water quality parameter that can be readily measured (Binding et al., 2007). Almost all SDD retrieval algorithms developed by previous studies for lake waters are empirical (Mouw et al., 2015; Olmanson et al., 2008). Lee et al. (2016) recently developed a semi-analytical algorithm to estimate SDD, but this algorithm is only for coastal waters. Nutrients cannot be directly retrieved from remote sensing data because they have no optical responses. Their retrieval algorithms were developed depending on the relationships between nutrients and optically active constituents, such as Chl*a* and TSM (Kutser et al., 1995; Song et al., 2012; Sun et al., 2013). Therefore, developing retrieval algorithms for water trophic indexes in lakes with high transferability is still challenging.

Several studies have attempted to employ remote sensing technology to assess lake TSI, which greatly limits traditional approaches (Matthews et al., 2012; Sass et al., 2007; Sheela et al., 2011; Song et al., 2012; Thiemann and Kaufmann, 2000; Watanabe et al., 2015; Wezernak et al., 1976). Wezernak et al. (1976) demonstrated that remote sensing technology has great potential for assessing the water TSI of inland waters and discussed the concept, framework and structure of TSI remote sensing for the first time. Olmanson et al. (2008) built a 20-year SDD database of Minnesota's 10,000 lakes using Landsat imagery and then assessed the variations in TSI based on the remotely estimated SDD from 1985 to 2005 for these lakes. Thiemann and Kaufmann (2000) assessed the TSI of five lakes in the Mecklenburg Lake District (Germany) using Chl*a* values determined from Indian Remote Sensing (IRS) LISS III data. Similarly, Watanabe et al. (2015) evaluated the TSI of the Barra Bonita Hydroelectric reservoir by means of Chl*a* derived from Landsat 8 OLI imagery. Sheela et al. (2011) attempted to assess the TSI of a lake system based on SDD and Chl*a* estimated from IRS LISS III imagery, suggesting that TSI based on SDD can provide an accurate prediction of the trophic status of a lake. Song et al. (2012) separately estimated the three trophic indicators (Chl*a*, SDD, and TP) from airborne imaging data and subsequently assessed the TSI of three central Indiana reservoirs synthetically using the estimated trophic indicators.

In summary, these previous studies that analyzed the TSI of lake waters by employing remote sensing data were based on indirect approaches, i.e., one or more water trophic indicators (Chl*a*, SDD, TP and TN) were first derived from remote sensing data, and then TSI was calculated and assessed. Thus, the studies have several limitations. First, larger uncertainties could result from indirect approaches than direct approaches due to the limited precision of the remote estimation of TSI-related water quality parameters (Odermatt et al., 2012; Olmanson et al., 2008; Sass et al., 2007; Song et al., 2012; Watanabe et al., 2015). Second, due to the high complexity of optical properties in inland waters, the algorithms for remotely estimating these TSI-related parameters are mostly based on empirical approaches; thus, the transferability of TSI assessments using remote sensing data is substantially limited (Babin et al., 2003; Shi et al., 2013). Therefore, it is urgent and necessary to develop an alternative scheme for rapidly assessing lake TSI through surrogate indexes that can be monitored relatively conveniently and quickly at an increased temporal and spatial resolution.

The light absorption coefficients of optically active constituents (OACs) in inland waters are essential variables that determine the optical variations and apparent optical properties of natural waters (Babin et al., 2003). OACs generally refer to phytoplankton biomass (Chl*a*), non-algal particles (NAP), and chromophoric dissolved organic matter (CDOM), which are closely related to variables for TSI assessment (Gupta, 2014; Shi et al., 2013). Variations in light absorption can physically reflect comprehensive information about OACs, directly rely on the concentration, composition, and size of OACs and have been modeled as functions of OAC concentrations, which is essential for the development of analytical and semi-analytical algorithms for the remote sensing of inland waters (Dall'Olmo et al., 2013). Thus, the light absorption coefficient can be reasonably considered an indicator of TSI, and our hypothesis is that TSI can be quantified from the light absorption coefficients of OACs.

Therefore, the main aims of this study are to: (1) model the relationship between TSI and the light absorption coefficients of OACs in inland waters, (2) calibrate and validate a semi-analytical approach for the remote sensing of TSI based on Landsat 8 OLI data, and (3) demonstrate an application of the developed approach in Lake Qiandaohu.

2. Materials and methods

2.1. Study areas and water sampling

From 2004 to 2018, a total of 812 water samples were collected from 27 lakes that ranged from oligotrophic to eutrophic, from shallow to deep, and from small to large in China (Fig. 1), during multiple cruises in different seasonal conditions (Table S1). Notably, the 50 water samples collected from Lake Nam Co were only for validating the proposed semi-analytical approach because no absorption coefficients of OACs were measured in this lake. Located at different climatic zones, these sampling lakes are widely geographically distributed from Northeast (Heilongjiang Province) to Southwest China (Yunnan Province and the Tibet Plateau), with altitudes varying from lower than 10 m to higher than 4700 m.

At each sampling site, water at four depths (0 m, 0.5 m, 1 m, 1.5 m, and 2.0 m) was collected and evenly mixed together into a Niskin bottle with a volume of approximately 2.5 L. All of the water samples were stored in a cooler with a low temperature (4 °C) for preservation and were immediately transported to the lab for analysis within 4 h. Geographical information, including latitude, longitude, and altitude, was determined using a Global Position System (GPS) with a horizontal accuracy of 2.0 m.

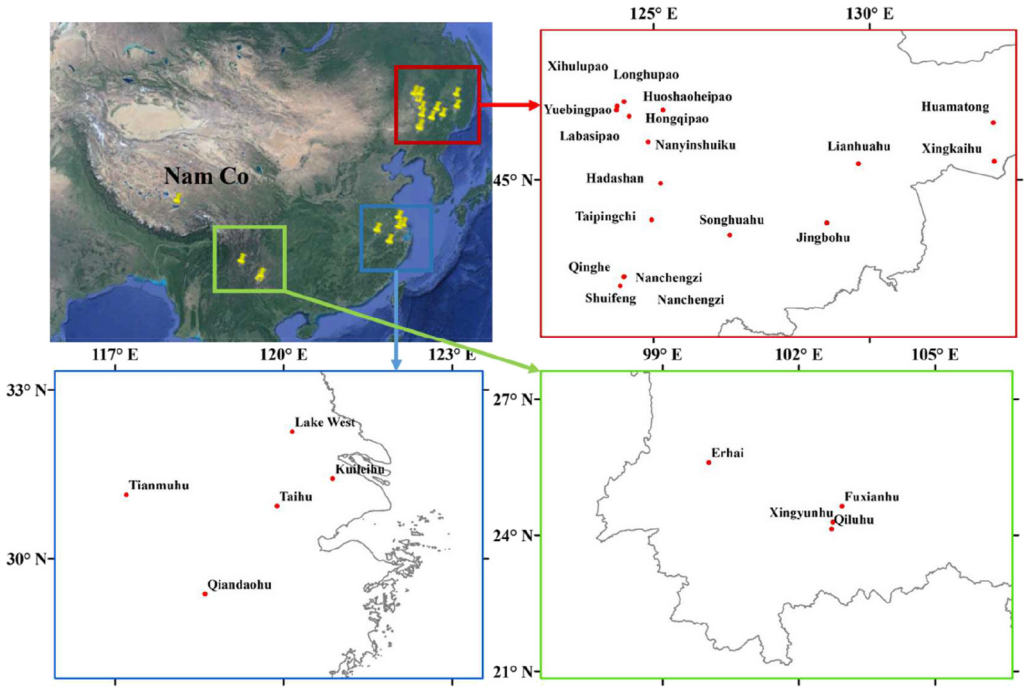

Fig. 1. Locations of the 27 sampling lakes.

2.2. Measurements of particle and CDOM absorption coefficients

The absorption coefficients of particles ($a_p(\lambda)$), phytoplankton ($a_{ph}(\lambda)$), and CDOM ($a_{CDOM}(\lambda)$) were measured in this study. The quantitative filter technique (QFT) was used to perform the measurements of $a_p(\lambda)$ and $a_{ph}(\lambda)$. We filtered 5–100 mL of each water sample through 25 mm diameter Whatman glassfiber GF/F filters under low vacuum pressure. The maximum optical density of particulate matter on the filters was set at 0.3. We positioned the filters in the sphere at a 100° angle from the beam and measured every 1 nm from 350 to 800 nm. We used a blank filter rinsed with Milli-Q water as a reference. We corrected all spectra using the mean value of the optical density between 750 and 800 nm to minimize differences between the sample and reference filters. A detailed description of the measurements of $a_p(\lambda)$ and $a_{ph}(\lambda)$ can be found in a previous study (Zhang et al., 2009). Before the $a_{CDOM}(\lambda)$ measurements were conducted, the water sample was filtered using a 47 mm diameter Whatman GF/F fiberglass filter with 0.7 μm pores to remove particulate matter, after which the sample was filtered through 0.22 μm cellulose membranes (Millipore) that had been prerinsed with 50 mL of Milli-Q water. The filtrate was collected in brown glass bottles that had been combusted at 450 °C for 6 h to remove any organic matter. The absorption of the filtrate was measured between 240 and 800 nm at 1 nm interval using a Shimadzu UV-2401PC spectrophotometer with a matching 4 cm quartz cuvette or UV–2550PC spectrophotometer with matching 5-cm quartz cells (Zhang et al., 2009). Thus, the total absorption of the OACs excluding pure water $a_{t\text{-}w}(\lambda)$ could be obtained from the sum of $a_p(\lambda)$, $a_{ph}(\lambda)$, and $a_{CDOM}(\lambda)$.

2.3. Measurements of biogeochemical parameters and trophic state assessment

The water biogeochemical parameters measured in this study were SDD, Chl*a*, TN, and TP. SDD was measured using a standard 30-cm diameter black and white quadrant Secchi disk. To measure Chl*a*, water samples (50–5000 mL, according to the amount of phytoplankton) were filtered through Whatman GF/F fiberglass filters. Chl*a* was extracted with ethanol (90%) at 80 °C and analyzed spectrophotometrically at 750 and 665 nm before and after acidification with 1 mol L^{-1} HCl with correction for phaeophytin-*a* (Simis et al., 2005; Sun et al., 2013). The TN and TP in the samples were examined by spectrophotometry after digestion with alkaline potassium persulfate according to the procedures for "Standard Methods for the Examination of Water and Wastewater" (Clesceri et al., 1989).

Carlson (1977) developed a numerical TSI based on Chl*a*, TP, or SDD that can be linked to the trophic state classification scheme to group lake waters into oligotrophic (TSI < 38), mesotrophic (48 > TSI > 38), eutrophic (61 > TSI > 49), and hypereutrophic (TSI > 61) categories. The trophic state of this study was assessed with the improved Carson's TSI based on four biogeochemical parameters, namely, Chl*a*, TN, TP, and SDD (Zhang et al., 2018). Specifically, TSI was calculated by the weighted mean method using the following six equations (Zhang et al., 2018):

$$TSI = \sum_{j=1}^{m} W_j * TSI(j) \quad (1)$$

$$W_j = R_j^2 / \sum_{i=1}^{m} R_{ji}^2 \quad (2)$$

$$TSI(Chla) = 10*(2.5 + 1.086*\ln(Chla)) \quad (3)$$

$$TSI(TP) = 10*(9.436 + 1.624*\ln(TP)) \quad (4)$$

$$TSI(TN) = 10*(5.453 + 1.694*\ln(TN)) \quad (5)$$

$$TSI(SDD) = 10*(5.118 + 1.94*\ln(SDD)) \quad (6)$$

where "m" is the number of parameters used for the TSI calculation (here m = 4); "R_j^2" is the determination coefficient between Chl*a* and the "j" parameter (here j = Chl*a*, and TP, TN, or SDD and $R^2_{Chla} = 1$; $R^2_{TP} = 0.55$; $R^2_{TN} = 0.23$; $R^2_{SDD} = 0.10$). Carlson (1977) justified that the best indicator of trophic status may vary regionally and temporarily. For example, TP could be chosen for the indicator only if TP is well correlated to Chl*a* (Carlson, 1977). In order to overcome this problem, the improved Carson's TSI synthetically uses several parameters to predict the water trophic status. W_j is adopted to assess the tightness between Chl*a* and other parameters. However, the limitation of the improved Carson's TSI is the determination of W_j. This is because W_j values may be different from lake to lake and also seasonally. Undoubtedly, it would add complexity of TSI calculation.

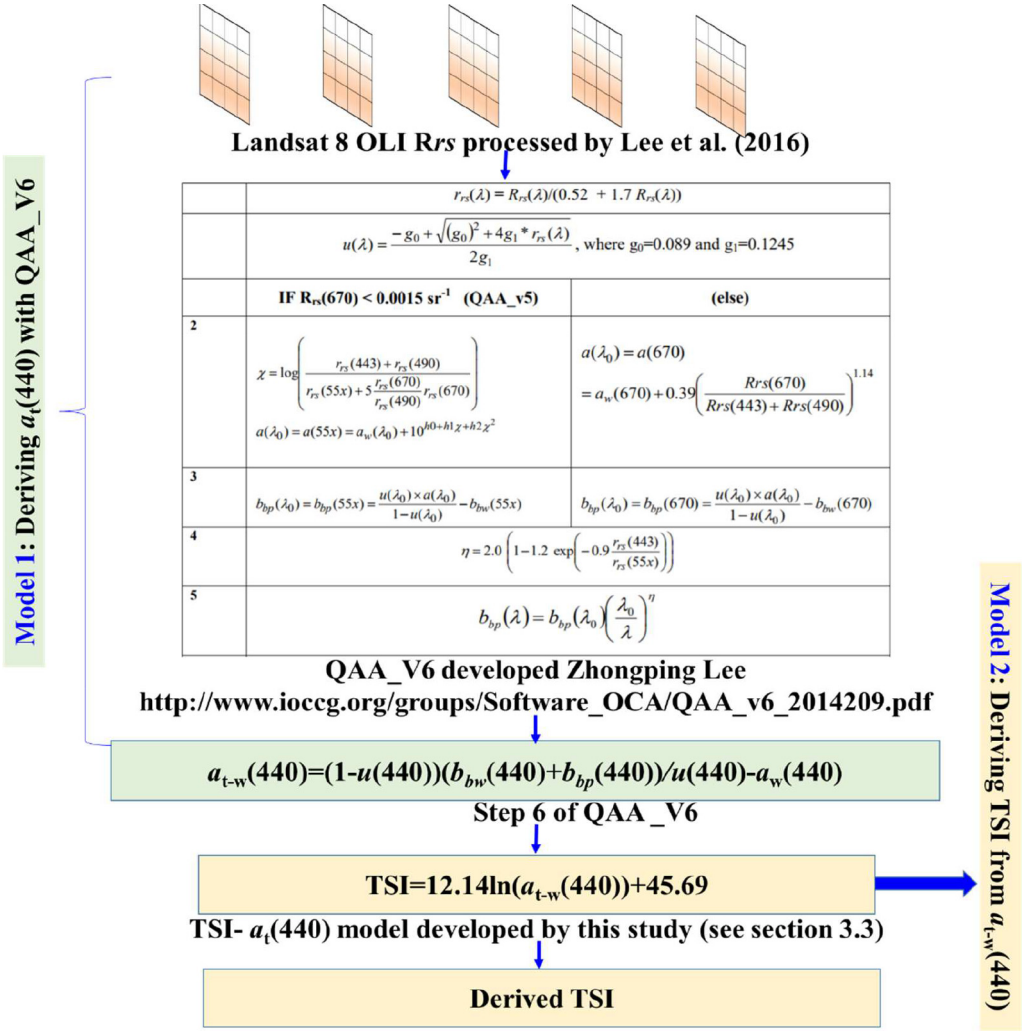

Fig. 2. Overall flowchart of the approach to semi-analytically derive TSI.

2.4. Landsat 8 OLI image acquisition and processing

To validate and address the applications of the proposed absorption-based model for TSI estimation for mapping the water trophic state using satellite data, twenty-one level-1 processed high-quality Landsat 8 OLI (OLI: the Operational Land Imager) images of Lake Qiandaohu (Zhejiang Province, China) covering the years from 2013 to 2017, one image of Lake Nam Co and one image of Lake Longhupao were downloaded from the United States Geological Survey (USGS) online site (http://glovis.usgs.gov/). The Landsat 8 OLI is a sun-synchronous orbiting satellite with an altitude of 705 km, an orbital inclination of 98.2°, a circle time of 98.8 min around the earth, and time and spatial resolutions that are consistent with Landsat 5 TM/Landsat 7 ETM+ (spatial resolution: 30 m, revisit interval: 16 days).

Deriving information about water environments from satellite imagery requires high-quality atmospheric corrections. The traditional atmospheric correction method (dark pixel method), primarily built for clean oceanic case-I waters, is not suitable for inland turbid waters because the dark pixel assumption of zero water-leaving radiance at the near-infrared is invalid (Wang and Shi, 2007). For inland turbid waters, Wang and Shi (2007) used a combination of NIR and shortwave-infrared (SWIR) bands to select the aerosol types, with all non-negligible water-leaving radiance extracted using an iterative method (Bailey et al., 2010), using NASA SeaWiFS Data Analysis System (SeaDAS) processing software (named the NASA standard approach) (Franz et al., 2015). Wei et al. (2018) concluded the NASA standard approach can generate reliable remote sensing reflectance (R_{rs}) products from Landsat 8 OLI data for coastal turbid waters. Here, we performed the NASA standard approach using SeaDAS (v7.4) for atmospheric correction to our acquired Landsat 8 OLI data. The main steps for the scheme are as follows, and specific details can be found in the studies of Franz et al. (2015) and Wei et al. (2018). (1) A look-up table of Rayleigh reflectance is prebuilt, and Rayleigh scattering can be determined from the look-up table (Franz et al., 2015; Wei et al., 2018). In addition, the contributions of glint and white caps are determined by sensor-specific spectral response functions and environmental conditions, such as pressure and wind speed (Franz et al., 2015). (2) Aerosol radiance is estimated using the method of Gordon and Wang (1994) with updated aerosol models developed from AERONET observations (Wei et al., 2018). To overcome the problem of the black pixel assumption in turbid waters, an iterative approach is applied to derive the aerosol radiance at the NIR and/or SWIR wavelengths (Wei et al., 2018). In this study, the combination of OLI bands 5 (865 nm) and 7 (2201 nm) was selected for Landsat 8 OLI data processing (Bailey et al., 2010). (3) The standard Level-2 quality flags (atmospheric correction failure, land pixel and probable cloud or ice) were masked (Wei et al., 2018); the on-orbit vicarious calibration was performed with a set of calibration gains extracted for Landsat 8 OLI data from the SeaDAS system (Franz et al., 2015).

To minimize the impacts of the temporal difference between the field and the selected Landsat 8 OLI images and considering that temporal variations of the biogeochemical parameters in Lake Nam Co

(oligotrophic lake), Lake Qiandaohu (oligotrophic to mesotrophic lake), and Lake Longhupao (eutrophic to hypereutrophic lake) are relatively weak, we set the criterion for matching satellite and in situ data to ≤3 days. Our criterion yielded a total of 128 matched pairs of Landsat 8 OLI $R_{rs}(\lambda)$ and in situ determined TSI values to validate our results. 50, 60 and 18 matched pairs were collected from Lake Nam Co, Lake Qiandaohu and Lake Longhupao, respectively. For these data pairs, we extracted the R_{rs} averaged from a 3 × 3 window of the Landsat 8 OLI images centered on each sampling point. These matching samples were distributed across the entire lake.

2.5. The overall approach to semi-analytically derive TSI

Overall, the semi-analytical approach for the remote sensing of TSI was established with two major steps: in the first step, the absorption coefficients of OACs ($a_{t\text{-}w}(\lambda)$) are estimated based on QAA_V6 from Landsat 8 OLI $R_{rs}(\lambda)$ (Model 1), and in the second step, the relationship between TSI and $a_{t\text{-}w}(\lambda)$ is modeled (Model 2) (Fig. 2).

For the first step, Landsat 8 OLI $R_{rs}(\lambda)$ information was fed into QAA_V6 to derive $a_{t\text{-}w}(\lambda)$ (Lee et al., 2016; Rodrigues et al., 2017) (Fig. 2). The QAA was has been widely applied to derive inherent optical parameters across various types of waters, including inland, coastal, and oceanic waters, because of its solid physical theoretical mechanism (Le et al., 2009; Mishra et al., 2013; Zheng et al., 2014). The approach has been improved and updated to the latest version (QAA_V6), with the target of enabling the application of this version in inland and coastal waters (http://www.ioccg.org/groups/Software_OCA/QAA_v6_2014209.pdf) (Lee et al., 2002, 2009, 2010, 2016). For the second step, a specific relationship equation between TSI and $a_{t\text{-}w}(\lambda)$ was constructed using in situ measured data (details can be found in Section 3.4).

2.6. Statistical analysis and accuracy assessment

Commercial Statistical Program for Social Sciences (SPSS) software (Version 17.0) was used to perform statistical analyses including calculations of the average, maximum, and minimum values, linear regressions and nonlinear regressions. We employed Pearson's correlation analysis to investigate the relationships between the variables. Significance levels were reported as significant ($p \le 0.05$) or not significant ($p > 0.05$). We assessed the accuracy of the developed model using the relative error (*RE*), mean absolute percent error (*MAPE*), and root-mean-square error (*RMSE*) between the measured and estimated values using the following equations:

$$RE = \frac{|Y_{measured} - Y_{estimated}|}{Y_{measured}} * 100\% \quad (7)$$

$$MAPE = \frac{1}{N}\sum_{i=1}^{N}\frac{|Y_{measured,i} - Y_{estimated,i}|}{Y_{measured,i}} * 100\% \quad (8)$$

$$RMSE = \sqrt{\frac{1}{N}\sum_{i=1}^{N}(Y_{\text{measured},i} - Y_{\text{estimated},i})^2} \quad (9)$$

where N is the number of samples, and Y_{measured} and $Y_{\text{estimated}}$ are the measured and estimated values, respectively.

3. Results

3.1. Biogeochemistry, TSI, and absorption coefficients

The sampling lakes (not including Lake Nam Co) spanned substantially ranges of nutrients, phytoplankton biomass, water clarity, trophic state, particle absorption, phytoplankton absorption and TSI (Table 1). TN, TP, Chl*a*, and SDD varied from 0.146 mg/L to 8.171 mg/L, from 0.001 mg/L to 0.493 mg/L, from 0.34 μg/L to 217.38 μg/L, from 0.07 m to 10.23 m, respectively. The absorption coefficients of OACs, namely, $a_{ph}(440)$, $a_p(440)$, and $a_{t\text{-}w}(440)$, ranged from 0.004 m^{-1} to 10.325 m^{-1}, from 0.010 m^{-1} to 12.980 m^{-1}, and from 0.010 m^{-1} to 14.196 m^{-1}, respectively. Phytoplankton, CDOM and NAP contributed 35%, 34% and 31% of $a_{t\text{-}w}(440)$, respectively. At 550 nm, NAP, phytoplankton, and CDOM contributed 63%, 29% and 8% of $a_{t\text{-}w}(550)$, respectively. At 675 nm, phytoplankton, NAP and CDOM contributed 65%, 33% and 2% of $a_{t\text{-}w}(675)$, respectively. The results highlight that the datasets contained varied water types ranging from particulate-dominated to CDOM-dominated waters. The maximal values of TN, TP, Chl*a*, and SDD were approximately 60, 493, 639, and 1461 times the minimal values, respectively. The ratios of the maximal values to minimal values of $a_{ph}(440)$, $a_p(440)$, and $a_{t\text{-}w}(440)$ were approximately 1234, 2468, and 1239, respectively. TSI varied from 15.66 to 85.88 exhibiting a substantial span from oligotrophic to eutrophic lakes. In addition, the average values of TN, TP, Chl*a*, and SDD were noticeably higher than the median values of TN, TP, Chl*a*, and SDD. Overall, our lake datasets covered a wide range of biogeochemical parameters and optical absorption properties, with TN, TP, Chl*a*, $a_{ph}(440)$, $a_p(440)$, and $a_{t\text{-}w}(440)$ varying by 1 to 4 orders of magnitude representing whole typical lakes from oligotrophic to hypereutrophic.

3.2. Modeling TSI using absorption coefficients of OACs

According to the sampling time and site, we evenly divided the 752 TSI absorption data pairs into two parts for model development and validation to ensure that the data of parts differed from each other with respect to either lakes or time. We attempted to use four types of functions, including linear, logarithmic, exponential and quadratic functions, to model the relationships between TSI and $a_{ph}(440)$, between TSI and $a_p(440)$, and between TSI and $a_{t\text{-}w}(440)$. The results showed that the logarithmic functions achieved the best precision for all three relationships, with the highest determination coefficients (Fig. 3(a–c)).

The validation results showed that all three models (TSI-$a_{ph}(440)$ model, TSI-$a_p(440)$ model, and TSI-$a_t(440)$ model) performed well in TSI estimation (Fig. 3(d–f)). Among them, the TSI-$a_{t\text{-}w}(440)$ model gave the best validation results with the lowest *RE* and *RMSE* values and the highest determination coefficients between in situ determined and estimated TSI. Nevertheless, the worst validation results were found for the TSI-$a_{ph}(440)$ model. The *RE* of the TSI-$a_{ph}(440)$ model for the validation dataset ranged from 0.06% to 57%, with a *MAPE* value of 16% and *RMSE* = 12.06; for the TSI-$a_p(440)$ model, *RE* varied from 0.02% to 51%, with a *MAPE* value of 12% and *RMSE* = 10.17; *RE* spanned from 0.01% to 45% for the TSI-$a_{t\text{-}w}(440)$ model, with a *MAPE* value of 6% and *RMSE* = 5.77.

The performance of the three models was also evaluated by the TSI retrieval *RE* distributions of the validation dataset (Fig. 4). For the *RE* values of TSI retrieved by the TSI-$a_{t\text{-}w}(440)$ model, there was no statistically significant relationship with in situ TSI; in addition, there were no statistically significant relationships between the *RE* values and other biogeochemical and absorption parameters, such as Chl*a*, TP, TN, SDD, and $a_{ph}(\lambda)$.

The results indicated that this model was robust and could be applied to all ranges of TSI retrieval; however, statistically significant relationships were found between the *RE* of TSI retrieved by the TSI-$a_{ph}(440)$ and TSI-$a_p(440)$ models and in situ TSI; for the TSI-$a_{ph}(440)$ model, the *RE* was especially high for 20 > TSI or TSI < 65 (*RE* > 30%), meaning that this model is only suitable for the waters with 20 < TSI < 65; in waters with TSI < 20, the *RE* of TSI-$a_{ph}(440)$ model was much > 30%, suggesting the TSI-$a_{ph}(440)$ model cannot be used for low-TSI retrieval with satisfactory performance.

Overall, the in situ determined TSI values exhibited good agreement with the TSI values estimated by the three types of models, with significant linear relationships (Fig. 3d, e, f). However, the TSI-$a_{ph}(440)$ model overestimates and underestimates TSI when TSI > 65 and

Table 1
The descriptive statistics of concentrations of total nitrogen (TN), total phosphorus (TP), chlorophyll *a* (Chl*a*), SDD, TSI, particle absorption ($a_{ph}(440)$), phytoplankton absorption ($a_p(440)$), and the OAC absorption coefficients ($a_{t\text{-}w}(440)$) for the whole collected dataset (752 samples). Note: Max, Min, and S.D. are abbreviations of maximum, minimum, and standard deviation.

Statistical variables	$a_p(440)$ (m^{-1})	$a_{ph}(440)$ (m^{-1})	$a_{t\text{-}w}(440)$ (m^{-1})	TSI	Chl*a* (μg/L)	TN (mg/L)	TP (mg/L)	SDD (m)
Max	12.98	10.32	14.19	85.87	217.38	8.17	0.493	10.23
Min	0.01	0.01	0.01	12.24	0.34	0.15	0.001	0.07
Mean	1.63	0.86	2.46	50.91	19.18	1.82	0.062	1.82
S.D.	2.17	0.84	2.35	15.65	26.92	1.41	0.066	2.05
Median	0.95	0.38	1.64	50.51	8.84	1.29	0.037	1.01

TSI < 20, respectively; when TSI > 65, the TSI-$a_p(440)$ model gave underestimated results. The in situ determined and estimated TSI values from the TSI-$a_{t\text{-}w}(440)$ model were evenly distributed along 1:1 lines (Fig. 3(f)) showing that TSI can modeled by total OAC absorption coefficients with satisfactory performance.

3.3. Validation of the semi-analytical approach

The semi-analytical approach was validated by deriving the TSI of three lakes with different trophic statuses, namely, oligotrophic Lake Nam Co, oligotrophic to mesotrophic Lake Qiandaohu, and eutrophic to hypereutrophic Lake Longhupao. A dataset of 128 sites containing concurrent measurements of in situ determined TSI and Landsat 8 OLI-derived R_{rs} values was used to evaluate the performance of the above-described approach (Fig. 2 in Section 2.5). The comparisons between the TSI derived by the approach with Landsat 8 OLI data and the in situ determined TSI are presented in Fig. 5.

Overall, the first approach performed well in the three water bodies. Specifically, for oligotrophic Lake Namco, the R^2 value of a linear regression analysis between the derived and in situ determined TSI is 0.75, with *RMSE* = 2.88, *MAPE* = 19% and an *RE* varying from 7% to 46% (Fig. 5(a)). For oli-mesotrophic Lake Qiandaohu, the R^2 value is

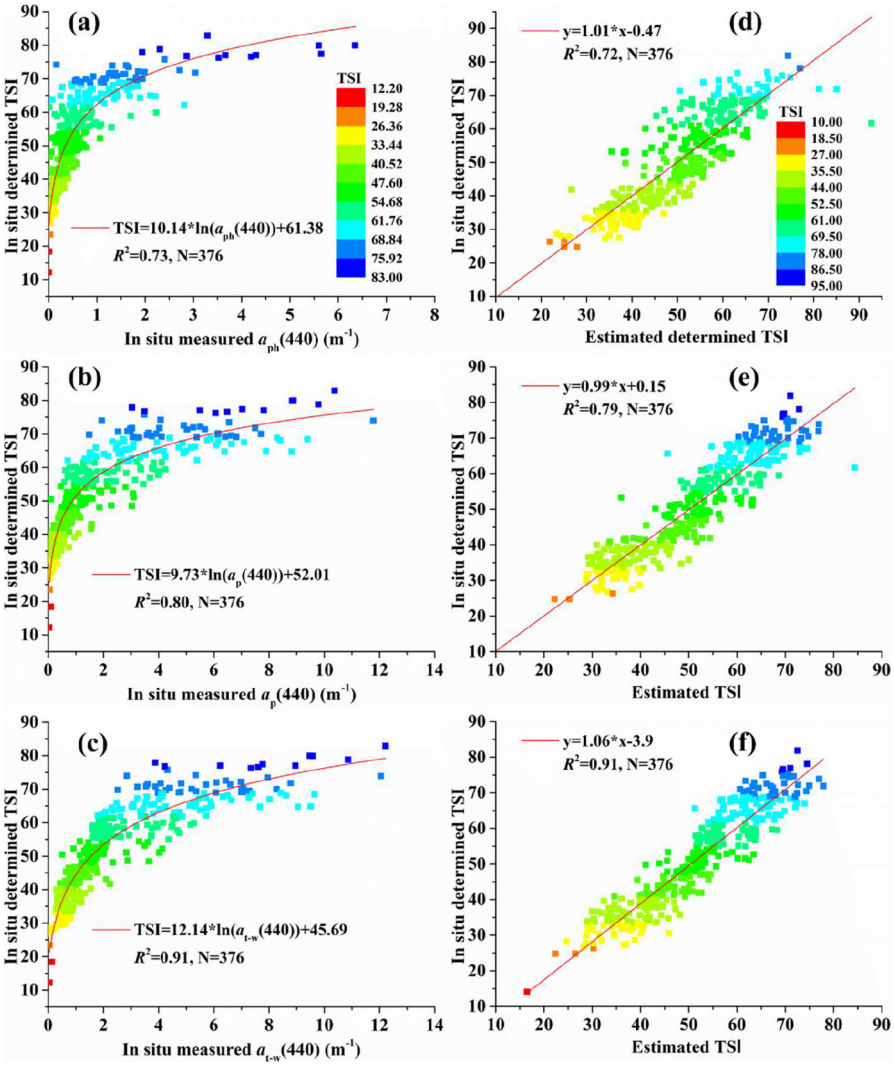

Fig. 3. Modeling the relationships between TSI and the absorption coefficients of $a_{ph}(440)$ (a), $a_p(440)$ (b) and $a_{t\text{-}w}(440)$ (c) and the relationships between in situ determined TSI and estimated TSI based on $a_{ph}(440)$ (d), $a_p(440)$ (e), and $a_{t\text{-}w}(440)$ (f).

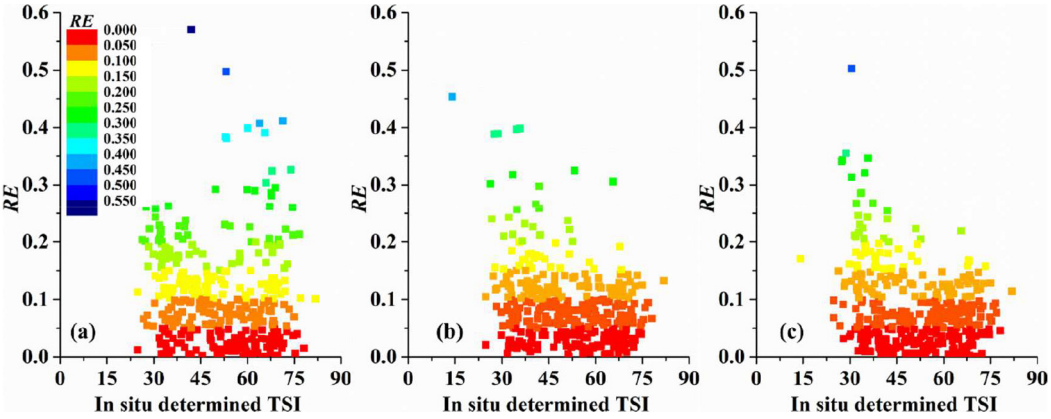

Fig. 4. *RE* distributions of TSI estimations using $a_{ph}(440)$ (a), $a_p(440)$ (b), and $a_{t\text{-}w}(440)$ (c).

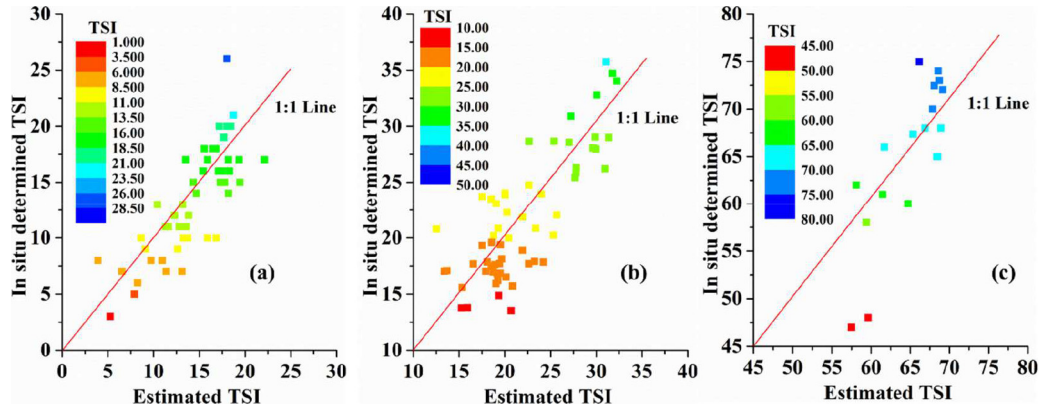

Fig. 5. Relationships between in situ determined TSI and satellite-derived TSI based on $a_{t\text{-}w}(440)$ in Lake Nam Co (a), Lake Qiandaohu (b) and Lake Longhupao (c).

0.70, with *RMSE* = 3.37, *MAPE* = 22% and an *RE* varying from 0.2% to 65% (Fig. 5(b)). Comparatively, the approach presented a relatively lower R^2 with 0.64 in hypereutrophic Lake Longhupao, the R^2 value is 0.64 although *MAPE* was only as 6% (*RMSE* = 5.23) (Fig. 5(c)). Thus, these results suggest the performance of the proposed semi-analytical scheme is robust and satisfactory in oliotrophic and mesotrophic inland waters.

3.4. Application of the semi-analytical approach in Lake Qiandaohu

The proposed approach was applied to the selected twenty-one Landsat 8 OLI images available from 2013 to 2017 to elucidate the temporal and spatial distribution of TSI in Lake Qiandaohu and subsequently to assess the trophic state of this lake. These Landsat 8 OLI images underwent atmospheric correction using the SeaDAS processing system (Franz et al., 2015).

The results showed obviously distinct temporal and spatial variability in the TSI of Lake Qiandaohu (Figs. 6–8). Overall, Lake Qiandaohu was characterized by relatively low TSI values, suggesting the low trophic levels in this lake from 2013 to 2017 (Fig. 6). Temporally, TSI ranged from 25.71 ± 3.52 to 34.33 ± 5.11 with the lowest average TSI of 25.71 ± 3.52 in December 2017, but the highest average TSI of 34.33 ± 5.11 in May 2015. The average TSI of 31.24 ± 4.56 in spring (March–May) was higher than that in the other three seasons (Fig. 7). In contrast, winter (December–February) showed the lowest average TSI of 26.61 ± 2.87. The average TSI in summer (June–August) and autumn (December–November) varied from 29.77 to 30.54, with a mean value of 30.28 ± 3.84, and from 27.31 to 31.02, with a mean value of 29.21 ± 4.99, respectively.

According to the TSI trophic state classification standards (Zhang et al., 2018), we assessed the trophic status of Lake Qiandaohu between 2013 and 2017 based on the derived TSI images. Only oligotrophic and mesotrophic were found in Lake Qiandaohu, and there were no eutrophic and hypereutrophic classes observed during the studied periods (Figs. 8 and 9–10). Overall, the oligotrophic class accounted for higher percentages (27% to 93%) of Lake Qiandaohu than the mesotrophic class. In December 2017 and May 2015, the percentages of the lake belonging to the oligotrophic class were the highest and lowest, respectively (Fig. 7). Seasonally, the oligotrophic class had the highest proportion in the winter (86%), coinciding with the dry season, and the lowest proportion in the spring (60%), coinciding with the wet season (Fig. 9). The proportions of the oligotrophic class in the summer and autumn were 63% and 71%, respectively. Spatially, 74% of Lake Qiandahu was ascribed to oligotrophic class, and 26% was ascribed to the mesotrophic class, mainly in small tributaries (Fig. 10).

Li et al. (2017) indicated that the nutrients in Lake Qiandaohu are mainly driven by rainfall. In the Lake Qiandaohu catchment, the rainfall in the spring was significantly higher than that in the other seasons. The amount of rainfall in the spring (176.7 mm) was approximately 2.6 times that in the winter (66.73 mm). The high loads of nutrients and sediment supplied by runoff in the wet spring season prompt more algal growth and decrease water clarity, resulting in an increase in the water trophic status (Li et al., 2018). On the other hand, there were significantly less nutrients and sediment in runoff a lower lake phytoplankton biomass in the dry winter season than in the spring, which jointly maintained the lower water trophic status in winter than in spring. In reservoirs, erosion by rainfall and runoff enhances increases in nutrients and sediment in inflowing streams, thus resulting in trophic status increases; this trend is reasonably expected and well documented (Rodrigues et al., 2017). Spatially, the TSI ranged from 11.50 to 40.12, with a mean value of 28.54 ± 3.50, for Lake Qiandaohu (Fig. 8). Generally, the TSI was < 21 near the shore, while TSI values > 31

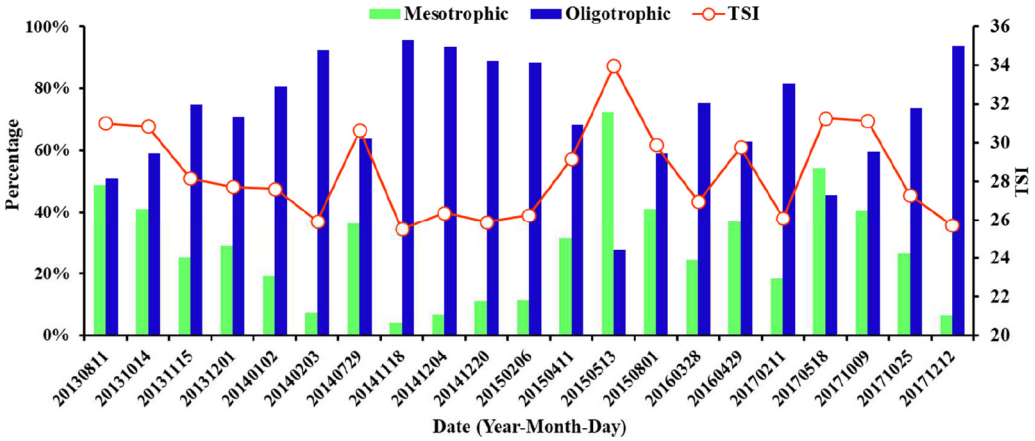

Fig. 6. Time series (2013–2017) of TSI and proportions of oligotrophic and mesotrophic classes in Lake Qiandaohu.

mostly appeared in the northwest and southwest areas of the water and in some small tributaries where Chl*a*, TP and TN were relatively high and water clarity was relatively low (Li et al., 2018, 2017). Incoming tributaries bring high nutrient levels (e.g., phosphorous and nitrogen) (Li et al., 2017) into the reservoir, which causes fast phytoplankton growth and prompts trophic state levels to increase. Our results were consistent with previous studies (Li et al., 2018; Li et al., 2017).

4. Discussion

4.1. Intrinsic relationships between OAC absorption and TSI

TSI represents a measurement of the bulk water quality and thus is a synthesized result of total suspended matter, phytoplankton and water nutrients. The relationships between TSI and its components indicate that TSI is mostly determined by SDD ($R^2 = 0.84$) and Chl*a* ($R^2 = 0.83$), followed by TP ($R^2 = 0.77$) and TN ($R^2 = 0.55$) (Fig. 11). Similarly, the absorption coefficients of OACs contain the compressive light absorption information of algal particles and NAP and CDOM directly reflecting phytoplankton biomass (Chl*a*), turbidity (SDD), and CDOM concentrations (Shi et al., 2013). The determination coefficients between Chl*a* and $a_{ph}(440)$, $a_p(440)$, and $a_{t\text{-}w}(440)$ were 0.61 ($p < 0.001$), 0.66 ($p < 0.001$), and 0.65 ($p < 0.001$), respectively; the determination coefficients of SDD correlated with these absorption coefficients were 0.70 ($p < 0.001$), 0.46 ($p < 0.001$), and 0.84 ($p < 0.001$). Seemingly, the absorption coefficients of OACs do not involve information about nutrients (TP and TN). However, the concentrations of nutrients are directly or indirectly related to phytoplankton biomass, total suspended matter and CDOM.

It has been recognized that TP loading is generally highly correlated with total suspended matter, which dominates particle absorption and thus determines water clarity in inland waters (Song et al., 2012; Wang et al., 2009). A significant correlation between TP and $a_{t\text{-}w}(440)$ was found for our dataset ($R^2 = 0.70$, $P < 0.001$). In addition, TP was closely related to Chl*a* in our dataset ($R^2 = 0.55$, $P < 0.005$). CDOM is an important optically active matter in aquatic ecosystems and affects

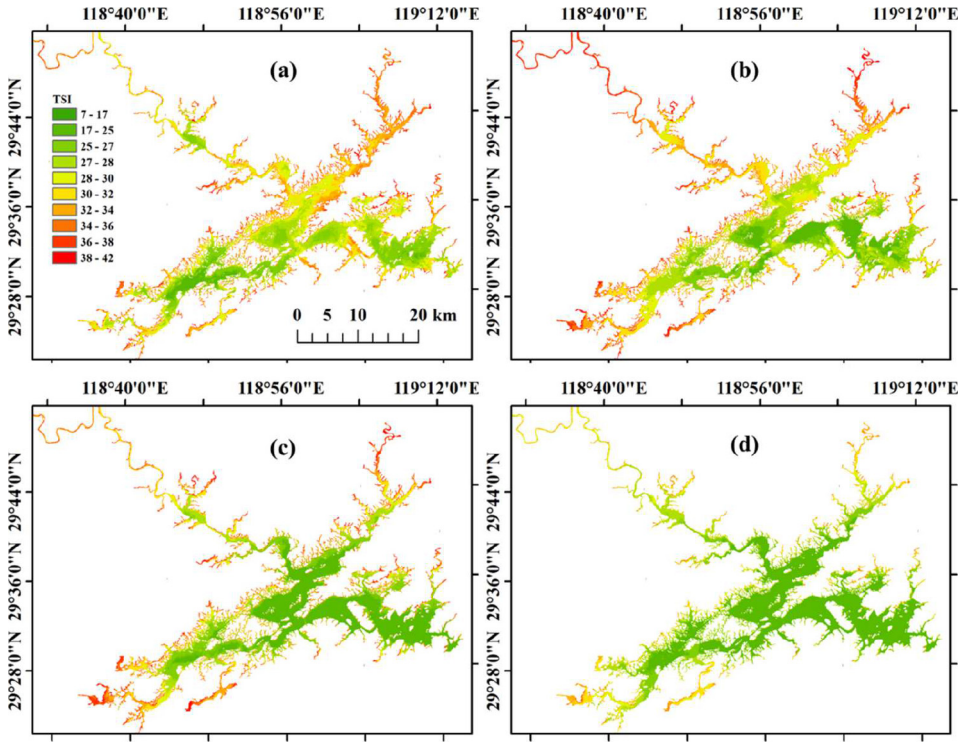

Fig. 7. Seasonal TSI distributions of Lake Qiandaohu. “a”, “b”, “c”, and “d” are “spring”, “summer”, “autumn”, and “winter”, respectively.

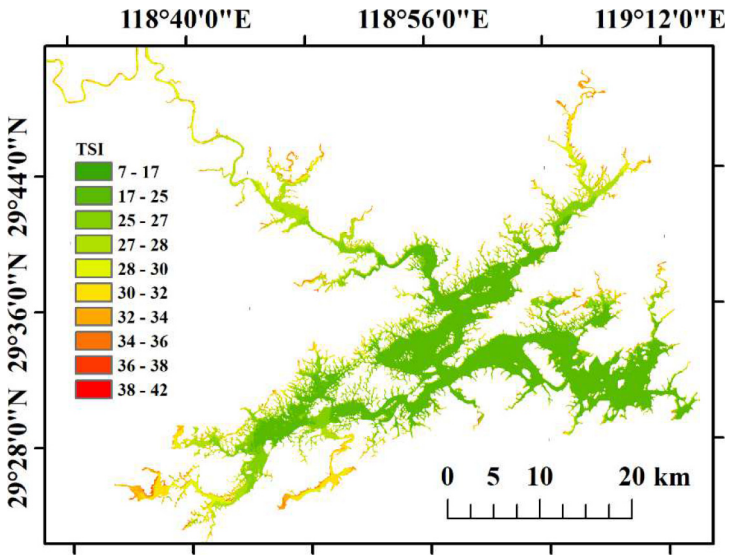

Fig. 8. Spatial distribution of TSI averaged from all estimated TSI values of the Landsat 8 OLI images from 2013 to 2017.

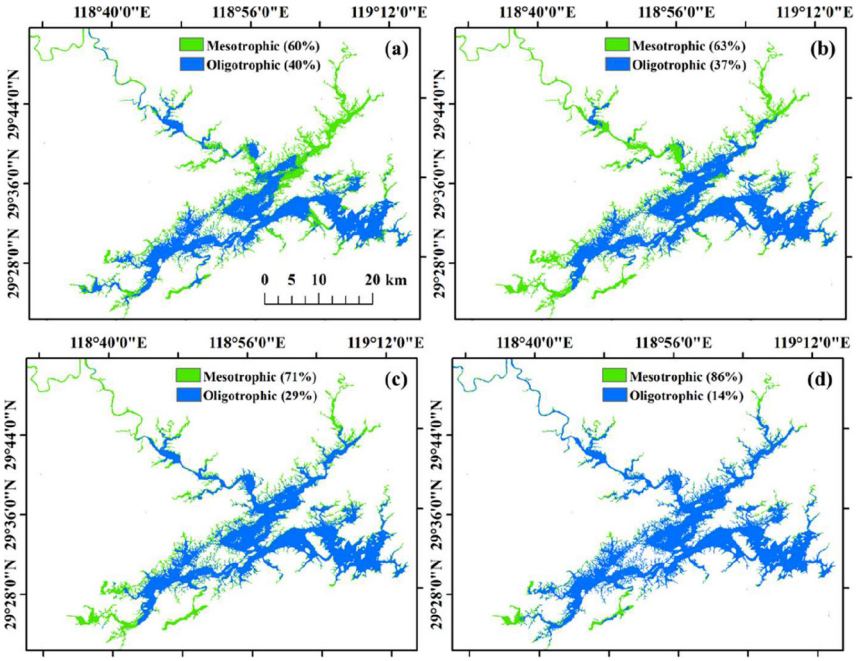

Fig. 9. Seasonal distributions of different trophic statuses in Lake Qiandaohu. “a”, “b”, “c”, and “d” are “spring”, “summer”, “autumn”, and “winter”, respectively.

ultraviolet radiation and thus carbon and nutrient cycling (Coble, 2007). Some studies have shown that as an important water color parameter, it is closely linked to nutrients (Webster et al., 2008; Zhang et al., 2018). Absorption coefficients of OACs can not only characterize water color parameters but also provide water nutrient information. Therefore, the absorption coefficients of OACs involve all information of TSI ingredients and therefore reasonably reflect water TSI.

4.2. Advantages and limitations of the proposed scheme

A large number of reports have been performed to demonstrate TSI assessment using in situ data and remote sensing methods (Olmanson et al., 2008; Sass et al., 2007; Song et al., 2012; Sun et al., 2013). Because the analysis of most TSI components must be performed in the lab, a TSI assessment based on in situ data cannot provide TSI information at large spatial and temporal scales and cannot be performed in real time, especially for large water bodies. Remote sensing TSI assessments can be summarized into two types. Type I is the computation of TSI based on the remote sensing estimation of a TSI parameter, such as SDD or Chl*a*. This method is simple and easy to implement, but any eutrophic state derived from simple parameters of SDD, Chl*a*, TP, or TN is biased, and the averaged TSI is more objective for inland waters than for other waters (Song et al., 2012). In addition, it is difficult to obtain satellite SDD and Chl*a* products with high accuracy, and retrievals of TP and TN from remote sensing data remain a great challenge in inland waters (Odermatt et al., 2012; Palmer et al., 2015). In type II assessments, TSI is compressively assessed based on remote sensing estimations of almost all TSI-needed parameters. The methods used for deriving the TSI parameters are mostly based on empirical or semi-empirical data, and the datasets used are very limited to one or more regions. Considering the complexity of optical properties in inland waters, the transferability of the methods becomes problematic. The present study proposed an alternative method to construct a scheme for remote-sensing-assessed TSI based on the absorption properties of

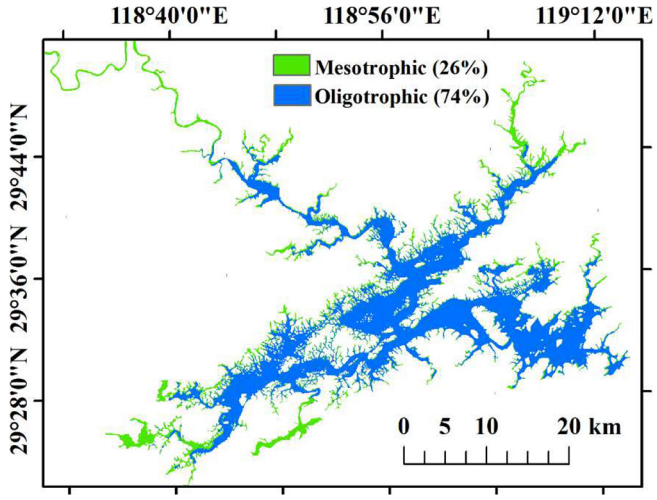

Fig. 10. Spatial distribution of different trophic statuses classified from all estimated TSI values of the Landsat 8 OLI images from 2013 to 2017.

water OACs. Given that both absorption coefficients and TSI are the compressive results of water quality properties, this study made a great attempt to utilize the absorption coefficients of water OACs for TSI assessment via remote sensing by deriving the absorption coefficients of water OACs from remote sensing data.

Compared to the traditional methods of TSI assessment (Matthews et al., 2012; Olmanson et al., 2008; Song et al., 2012; Thackeray et al., 2016), our proposed scheme has the following advantages. First, the use of a large in situ dataset ensures the robustness and validity of the proposed scheme. The substantially large dataset explored here provided a unique opportunity to establish the general relationship between the absorption coefficients of water OACs and TSI with sufficiently strong validity and robustness. Second, from the perspective of remote sensing applications, the proposed model can reduce cumulated errors as much as possible and can enhance the method transferability for the remote sensing of TSI. Traditionally, parameters such as Chl*a*, SDD, TN, and TP must be derived from remote sensing data separately in order to retrieve TSI, which leads to the accumulation of corresponding errors (Chl*a*, SDD, TN, and TP) and increased uncertainty in the TSI results. Using only remotely sensed $a_{t\text{-}w}(440)$ to reasonably replace these TSI-needed parameters can decrease the uncertainty of TSI values derived based on traditional methods. In addition, it is known that inherent optical properties (IOPs) remote sensing estimation is much easier and more accurate than that of water constituents in inland waters (Lee et al., 2002; Shi et al., 2013). In inland waters, the specific absorption coefficients of water constituents are largely varied, which greatly affects the water constituents' derived from IOP data, thus resulting in errors in the water constituents' retrievals based on quasi-analytical or analytical methods (Shi et al., 2013). However, the retrieval $a_{t\text{-}w}(440)$ is directly used for TSI assessment, which avoids errors resulting from large variations in the specific absorption coefficients of water constituents. $a_{t\text{-}w}(440)$ can be easily and directly derived from remote sensing data using quasi-analytical or analytical methods, and our proposed model can avoid the variations of specific absorption coefficients, both of which enhance the scheme transferability. Recently, a type of global TSI product was released by the Copernicus Land Service (https://land.copernicus.eu/global/products/lwq); however, the TSI products were generated solely from one parameter (Chl*a*) derived from MERIS or Sentinel OLCI data. Presently, there is no algorithm that can accurately estimate Chl*a* from remote sensing data for global inland waters due to high complexity of their optical properties (Shi et al., 2013).

However, the proposed approach has the following two limitations. First, the TSI-$a_{t\text{-}w}(440)$ model cannot be applied to most lakes in boreal zones. In the majority of boreal lakes, the absorption of CDOM is generally very high, thus dominating the variability of optical properties in these waters, especially at low wavelengths (Kutser et al., 2005). The percent contribution of CDOM to the total absorption ranged from 48% to 99% at 442 nm in 15 boreal lakes of southern Finland, whereas the contributions of other OACs varied fairly consistently from < 1% to 34% (Ylöstalo et al., 2014). In addition, the proportion of humic-like substances is relatively high in boreal lakes, and 80% of CDOM in boreal lakes originates from the materials from forest litter

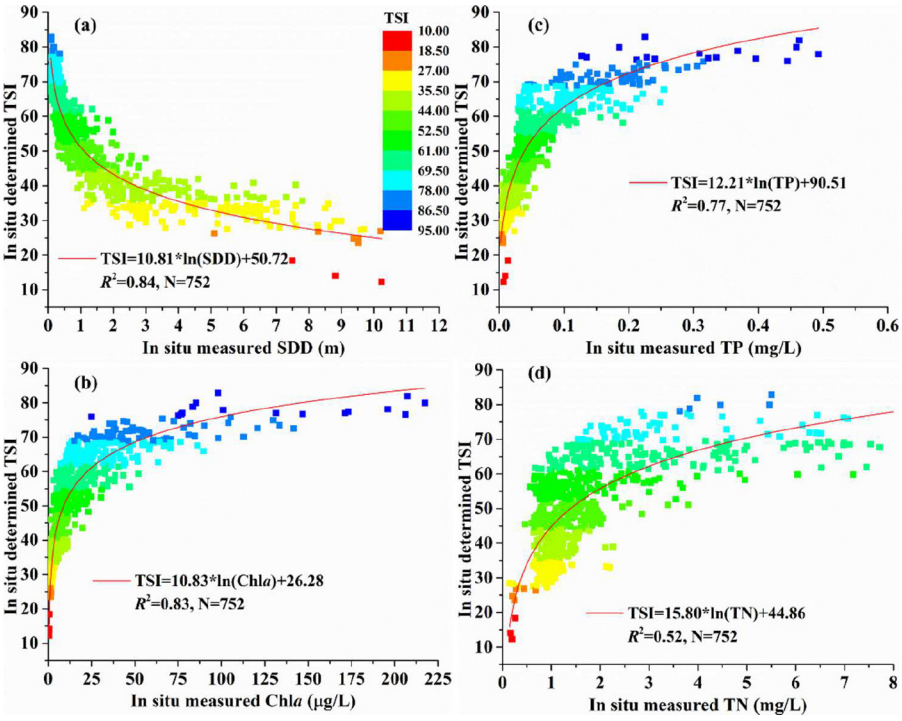

Fig. 11. Relationships between TSI and SDD (a), Chl*a* (b), TP (c), and TN (d).

decomposition and soil column leaching in lake catchments (Kellerman et al., 2014; Kothawala et al., 2014). This indicates that correlations of CDOM to Chl*a* and nutrients are usually weak; thus, $a_{t\text{-}w}(440)$ dominated by CDOM does not reflect the water trophic status, eventually invalidating the proposed approach in the remote sensing of TSI for boreal lakes. Nevertheless, this does not mean that the approach cannot be applied to all waters dominated by CDOM. If, in lakes similar to our study areas, CDOM derived from phytoplankton degradation and agricultural or urban pollutants, is therefore closely associated with TSI (Zhou et al., 2018).

Second, our approach may have large uncertainty for waters with high suspended sediment concentrations. In waters with high suspended sediment concentrations, the water-leaving radiance is dominated by particulate scattering properties, not absorption (Doxaran et al., 2002). Therefore, the water volume scattering coefficient is the best way to imply suspended sediment concentrations among these IOPs (Lubac and Loisel, 2007; Nechad et al., 2010). Due to data unavailability and difficulties in partitioning water volume scattering into individuals (phytoplankton and suspended sediment scattering), scattering was not considered in modeling the relationships between TSI and IOPs in this study. However, $a_{t\text{-}w}(440)$ is usually co-controlled by CDOM and phytoplankton, not suspended sediments, so $a_{t\text{-}w}(440)$ cannot fully reflect information on suspended sediments (Shi et al., 2013; Xue et al., 2017). Furthermore, scattering coefficients can also influence the accuracy of derivations of $a_{t\text{-}w}(440)$ by QAA_V6; high scattering coefficients will result in more errors in the derived $a_{t\text{-}w}(440)$ (Lee et al., 2010; Rodrigues et al., 2017).

5. Conclusions

In this study, we established a semi-analytical approach to remotely assess TSI based on Landsat 8 OLI data for inland waters by combining the two models: QAA_V6 and the relationship between TSI and the total absorption of OACs. This approach can overcome the drawbacks of traditional methods of TSI assessment that use a single remotely sensed TSI ingredient (Chl*a* or SDD). The validation results demonstrated a certain transferability and thereby suggested that the approach can be used to derive the TSI of oligo- to hypereutrophic inland waters. We applied the approach to the selected twenty-one Landsat 8 OLI images available from 2013 to 2017 to obtain the temporal and spatial distribution of TSI for Lake Qiandaohu and to subsequently assess the trophic state of this lake.

However, the proposed approach cannot be applied to assess the TSI of boreal lakes wherein waters are dominated by CDOM. In boreal lakes, the weak correlations of CDOM to Chl*a* and nutrients lead to errors in deriving TSI from $a_{t\text{-}w}(440)$. In addition, some uncertainties may be produced when using the approach in waters dominated by suspended sediments. Therefore, in future work, scattering should be considered in the TSI-$a_{t\text{-}w}(440)$ model to make our approach suitable for more waters. We validated the approach using these lakes (not including Lake Nam Co) which also were used for constructing TSI-$a_{t\text{-}w}(440)$ model, meaning that it is necessary to test the approach validation in other waters with similar characteristics as this study in future work. We encourage more datasets in more water bodies worldwide to further validate and improve our approach. In addition, more quasi-analytical or analytical methods combining various satellite data (Sentinel OLCI, MODIS data, etc.) could be developed for deriving $a_{t\text{-}w}(440)$ to couple the TSI-$a_{t\text{-}w}(440)$ model.

Supplementary data to this article can be found online at https://doi.org/10.1016/j.rse.2019.111349.

Acknowledgments

This study was supported by grants from the National Natural Science Foundation of China (Nos. 41771472 and 41621002), the Youth Innovation Promotion Association CAS (2017365), the Key Research Program of Frontier Sciences of the Chinese Academy of Sciences (QYZDB-SSW-DQC016), the “Strategic Priority Research Program” of the Chinese Academy of Sciences (XDA19070301), and “One-Three-Five” Strategic Planning of Nanjing Institute of Geography and Limnology, Chinese Academy of Sciences (NIGLAS2017GH03). The authors thank all the members for their participation in the field experiments. Our deepest gratitude goes to the three anonymous reviewers for their careful work and thoughtful suggestions that have helped improve this paper substantially.

References

Babin, M., Stramski, D., Ferrari, G.M., Claustre, H., Bricaud, A., Obolensky, G., Hoepffner, N., 2003. Variations in the light absorption coefficients of phytoplankton, nonalgal particles, and dissolved organic matter in coastal waters around Europe. J. Geophys. Res. Oceans 108. https://doi.org/10.1029/2001jc000882.

Bailey, S.W., Franz, B.A., Werdell, P.J., 2010. Estimation of near-infrared water-leaving reflectance for satellite ocean color data processing. Opt. Express 18, 7521–7527.

Binding, C.E., Jerome, J.H., Bukata, R.P., Booty, W.G., 2007. Trends in water clarity of the lower Great Lakes from remotely sensed aquatic color. J. Great Lakes Res. 33, 828–841.

Carlson, R.E., 1977. A trophic state index for lakes. Limnol. Oceanogr. 22, 361–369.

Clesceri, A., Greenberg, E., Trussel, R., 1989. Standard Methods: For the Examination of Water and Waste Water, 17th ed. American Public Health Association, Washington.

Coble, P.G., 2007. Marine optical biogeochemistry: the chemistry of ocean color. Cheminform 107, 402.

Dall'Olmo, G., Gitelson, A.A., Rundquist, D.C., 2003. Towards a unified approach for remote estimation of chlorophyll-a in both terrestrial vegetation and turbid productive waters. Geophys. Res. Lett. 30, 159–171.

Dodds, W.K., 2007. Trophic state, eutrophication and nutrient criteria in streams. Trends Ecol. Evol. 22, 669–676.

Doxaran, D., Froidefond, J.M., Lavender, S., Castaing, P., 2002. Spectral signature of highly turbid waters: application with SPOT data to quantify suspended particulate matter concentrations. Remote Sens. Environ. 81, 149–161.

Franz, B.A., Bailey, S.W., Kuring, N., Werdell, P.J., 2015. Ocean color measurements with the Operational Land Imager on Landsat-8: implementation and evaluation in SeaDAS. J. Appl. Remote. Sens. 9. https://doi.org/10.1117/1.JRS.9.096070.

Gons, H.J., Auer, M.T., Effler, S.W., 2008. MERIS satellite chlorophyll mapping of oligotrophic and eutrophic waters in the Laurentian Great Lakes. Remote Sens. Environ. 112, 4098–4106.

Gordon, H.R., Wang, M., 1994. Retrieval of water-leaving radiance and aerosol optical thickness over the oceans with SeaWiFS: a preliminary algorithm. Appl. Optics 33, 443–452.

Gower, J., King, S., Borstad, G., Brown, L., 2005. Detection of intense plankton blooms using the 709 nm band of the MERIS imaging spectrometer. Int. J. Remote Sens. 26, 2005–2012.

Gupta, M., 2014. A new trophic state index for lagoons. J. Ecosyst. 2014, 152473. https://doi.org/10.1155/2014/152473.

Hunter, P.D., Tyler, A.N., Willby, N.J., Gilvear, D.J., 2008. The spatial dynamics of vertical migration by Microcystis aeruginosa in a eutrophic shallow lake: a case study using high spatial resolution time-series airborne remote sensing. Limnol. Oceanogr. 53, 2391–2406.

Kaunzinger, C.M.K., Morin, P.J., 1998. Productivity controls food-chain properties in microbial communities. Nature 395, 495–497.

Kellerman, A.M., Dittmar, T., Kothawala, D.N., Tranvik, L.J., 2014. Chemodiversity of dissolved organic matter in lakes driven by climate and hydrology. Nat. Commun. 5. https://doi.org/10.1038/ncomms4804.

Kothawala, D.N., Stedmon, C.A., Müller, R.A., Weyhenmeyer, G.A., K?Hler, S.J., Tranvik, L.J., 2014. Controls of dissolved organic matter quality: evidence from a large-scale boreal lake survey. Glob. Chang. Biol. 20, 1101–1114.

Kutser, T., 2004. Quantitative detection of chlorophyll in cyanobacterial blooms by satellite remote sensing. Limnol. Oceanogr. 49, 2179–2189.

Kutser, T., Arst, H., Miller, T., Kã, Ã., Rmann, L., Milius, A., 1995. Telespectrometrical estimation of water transparency, chlorophyll-a and total phosphorus concentration of Lake Peipsi. Int. J. Remote Sens. 16, 3069–3085.

Kutser, T., Pierson, D.C., Kallio, K.Y., Reinart, A., Sobek, S., 2005. Mapping lake CDOM by satellite remote sensing. Remote Sens. Environ. 94, 535–540.

Le, C.F., Li, Y.M., Zha, Y., Sun, D.Y., Yin, B., 2009. Validation of a Quasi-Analytical Algorithm for highly turbid eutrophic water of Meiliang Bay in Taihu Lake, China. IEEE Trans. Geosci. Remote Sens. 47, 2492–2500.

Lee, Z., Carder, K.L., Arnone, R.A., 2002. Deriving inherent optical properties from water color: a multiband quasi-analytical algorithm for optically deep waters. Appl. Opt. 41, 5755.

Lee, Z., Lubac, B., Werdell, J., Arnone, R., 2009. An Update of the Quasi-Analytical Algorithm (QAA_v5). www.ioccg.org/groups/Software_OCA/QAA_v5.pdf.

Lee, Z., Shang, S., Hu, C., Lewis, M., Arnone, R., Li, Y., Lubac, B., 2010. Time series of bio-optical properties in a subtropical gyre: implications for the evaluation of interannual trends of biogeochemical properties. J. Geophys. Res. Oceans 115. https://doi.org/10.1029/2009JC005865.

Lee, Z., Shang, S., Qi, L., Yan, J., Lin, G., 2016. A semi-analytical scheme to estimate Secchi-disk depth from Landsat-8 measurements. Remote Sens. Environ. 177, 101–106.

Li, Y., Zhang, Y., Shi, K., Zhu, G., Zhou, Y., Zhang, Y., Guo, Y., 2017. Monitoring spatiotemporal variations in nutrients in a large drinking water reservoir and their relationships with hydrological and meteorological conditions based on Landsat 8 imagery. Sci. Total Environ. 599–600, 1705–1717.
Li, Y., Zhang, Y., Shi, K., Zhou, Y., Zhang, Y., Liu, X., Guo, Y., 2018. Spatiotemporal dynamics of chlorophyll-a in a large reservoir as derived from Landsat 8 OLI data: understanding its driving and restrictive factors. Environ. Sci. Pollut. Res. 25, 1359–1374.
Lubac, B., Loisel, H., 2007. Variability and classification of remote sensing reflectance spectra in the eastern English Channel and southern North Sea. Remote Sens. Environ. 110, 45–58.
Matthews, M.W., Bernard, S., Robertson, L., 2012. An algorithm for detecting trophic status (chlorophyll-a), cyanobacterial-dominance, surface scums and floating vegetation in inland and coastal waters. Remote Sens. Environ. 124, 637–652.
Mishra, S., Mishra, D.R., Lee, Z., Tucker, C.S., 2013. Quantifying cyanobacterial phycocyanin concentration in turbid productive waters: a quasi-analytical approach. Remote Sens. Environ. 133, 141–151.
Mouw, C.B., Greb, S., Aurin, D., Digiacomo, P.M., Lee, Z., Twardowski, M., Binding, C., Hu, C., Ma, R., Moore, T., 2015. Aquatic color radiometry remote sensing of coastal and inland waters: challenges and recommendations for future satellite missions. Remote Sens. Environ. 160, 15–30.
Nechad, B., Ruddick, K.G., Park, Y., 2010. Calibration and validation of a generic multisensor algorithm for mapping of total suspended matter in turbid waters. Remote Sens. Environ. 114, 854–866.
Odermatt, D., Gitelson, A., Brando, V.E., Schaepman, M., 2012. Review of constituent retrieval in optically deep and complex waters from satellite imagery. Remote Sens. Environ. 118, 116–126.
Olmanson, L.G., Bauer, M.E., Brezonik, P.L., 2008. A 20-year Landsat water clarity census of Minnesota's 10,000 lakes. Remote Sens. Environ. 112, 4086–4097.
Pace, M.L., Batt, R.D., Buelo, C.D., Carpenter, S.R., Cole, J.J., Kurtzweil, J.T., Wilkinson, G.M., 2017. Reversal of a cyanobacterial bloom in response to early warnings. Proc. Natl. Acad. Sci. U. S. A. 114, 352–357.
Palmer, S.C.J., Kutser, T., Hunter, P.D., 2015. Remote sensing of inland waters: challenges, progress and future directions. Remote Sens. Environ. 157, 1–8.
Pekel, J.F., Cottam, A., Gorelick, N., Belward, A.S., 2016. High-resolution mapping of global surface water and its long-term changes. Nature 540, 418–422.
Piao, S., Ciais, P., Friedlingstein, P., Peylin, P., Reichstein, M., Luyssaert, S., Margolis, H., Fang, J., Barr, A., Chen, A., 2008. Net carbon dioxide losses of northern ecosystems in response to autumn warming. Nature 451, 49–52.
Rodrigues, T., Alcantara, E., Watanabe, F., Imai, N., 2017. Retrieval of Secchi disk depth from a reservoir using a semi-analytical scheme. Remote Sens. Environ. 198, 213–228.
Ryan, J.P., Fischer, A.M., Kudela, R.M., Gower, J.F.R., King, S.A., Marin, R., Marin III, M., Chavez, F.P., 2009. Influences of upwelling and downwelling winds on red tide bloom dynamics in Monterey Bay, California. Cont. Shelf Res. 29, 785–795.
Sass, G.Z., Creed, I.F., Bayley, S.E., Devito, K.J., 2007. Understanding variation in trophic status of lakes on the Boreal Plain: a 20-year retrospective using Landsat TM imagery. Remote Sens. Environ. 109, 127–141.
Sheela, A.M., Letha, J., Joseph, S., Ramachandran, K.K., Sanalkumar, S.P., 2011. Trophic state index of a lake system using IRS (P6-LISS III) satellite imagery. Environ. Monit. Assess. 177, 575–592.
Shen, F., Zhou, Y.X., Li, D.J., Zhu, W.J., Salama, M.S., 2010. Medium resolution imaging spectrometer (MERIS) estimation of chlorophyll-a concentration in the turbid sediment-laden waters of the Changjiang (Yangtze) Estuary. Int. J. Remote Sens. 31, 4635–4650.
Shi, K., Li, Y., Li, L., Lu, H., 2013. Absorption characteristics of optically complex inland waters: implications for water optical classification. J. Geophys. Res. Biogeosci. 118, 860–874.
Simis, S.G.H., Peters, S.W.M., Gons, H.J., 2005. Remote sensing of the cyanobacterial pigment phycocyanin in turbid inland water. Limnol. Oceanogr. 50, 237–245.
Soliveres, S., van der Plas, F., Manning, P., Prati, D., Gossner, M.M., et al., 2016. Biodiversity at multiple trophic levels is needed for ecosystem multifunctionality. Nature 536, 456–459.
Song, K., Li, L., Li, S., Tedesco, L., Hall, B., Li, L., 2012. Hyperspectral remote sensing of total phosphorus (TP) in three central Indiana water supply reservoirs. Water Air Soil Pollut. 223, 1481.
Sun, D., Li, Y., Wang, Q., Gao, J., Le, C., Huang, C., Gong, S., 2013. Hyperspectral remote sensing of the pigment C-phycocyanin in turbid inland waters, based on optical classification. IEEE Trans. Geosci. Remote Sens. 51, 3871–3884.
Temmerman, S., Meire, P., Bouma, T.J., Herman, P.M., Ysebaert, T., De Vriend, H.J., 2013. Ecosystem-based coastal defence in the face of global change. Nature 504, 79–83.
Thackeray, S.J., Henrys, P.A., Hemming, D., Bell, J.R., Botham, M.S., et al., 2016. Phenological sensitivity to climate across taxa and trophic levels. Nature 535, 241–245.
Thiemann, S., Kaufmann, H., 2000. Determination of chlorophyll content and trophic state of lakes using field spectrometer and IRS-1C satellite data in the Mecklenburg lake district, Germany. Remote Sens. Environ. 73, 227–235.
Walsh, J.R., Carpenter, S.R., Vander Zanden, M.J., 2016. Invasive species triggers a massive loss of ecosystem services through a trophic cascade. Proc. Natl. Acad. Sci. U. S. A. 113, 4081–4085.
Wang, M.H., Shi, W., 2007. The NIR-SWIR combined atmospheric correction approach for MODIS ocean color data processing. Opt. Express 15, 15722–15733.
Wang, S., Stiles, T., Flynn, T., Stahl, A.J., Gutierrez, J.L., Angelo, R.T., Frees, L., 2009. A modeling approach to water quality management of an agriculturally dominated watershed, Kansas, USA. Water Air Soil Pollut. 203, 193–206.
Watanabe, F.S.Y., Alcantara, E., Rodrigues, T.W.P., Imai, N.N., Barbosa, C.C.F., Rotta, L.H.D., 2015. Estimation of chlorophyll-a concentration and the trophic state of the Barra Bonita Hydroelectric reservoir using OLI/Landsat-8 images. Int. J. Environ. Res. Public Health 12, 10391–10417.
Webster, K.E., Soranno, P.A., Cheruvelil, K.S., Bremigan, M.T., Downing, J.A., Vaux, P.D., Asplund, T.R., Bacon, L.C., Connor, J., 2008. An empirical evaluation of the nutrient-color paradigm for lakes. Limnol. Oceanogr. 53, 1137–1148.
Wei, J., Lee, Z., Garcia, R., Zoffoli, L., Armstrong, R.A., Shang, Z., Sheldon, P., Chen, R.F., 2018. An assessment of Landsat-8 atmospheric correction schemes and remote sensing reflectance products in coral reefs and coastal turbid waters. Remote Sens. Environ. 215, 18–32.
Wetzel, R.G., Likens, G.E., 2010. Limnological analyses. Lakes Reserv. Res. Manag. 7, 135.
Wezernak, C.T., Tanis, F.J., Bajza, C.A., 1976. Trophic state analysis of inland lakes. Remote Sens. Environ. 5, 147–164.
Xue, K., Zhang, Y., Duan, H., Ma, R., 2017. Variability of light absorption properties in optically complex inland waters of Lake Chaohu, China. J. Great Lakes Res. 43, 17–31.
Ylöstalo, P., Kallio, K., Seppälä, J., 2014. Absorption properties of in-water constituents and their variation among various lake types in the boreal region. Remote Sens. Environ. 148, 190–205.
Zhang, Y., van Dijk, M., Liu, M., Zhu, G., Qin, B., 2009. The contribution of phytoplankton degradation to chromophoric dissolved organic matter (CDOM) in eutrophic shallow lakes: field and experimental evidence. Water Res. 43, 4685–4697.
Zhang, Y., Zhou, Y., Shi, K., Qin, B., Yao, X., Zhang, Y., 2018. Optical properties and composition changes in chromophoric dissolved organic matter along trophic gradients: implications for monitoring and assessing lake eutrophication. Water Res. 131, 255–263.
Zheng, G., Stramski, D., Reynolds, R.A., 2014. Evaluation of the Quasi-Analytical Algorithm for estimating the inherent optical properties of seawater from ocean color: comparison of Arctic and lower-latitude waters. Remote Sens. Environ. 155, 194–209.
Zhou, Y., Davidson, T.A., Yao, X., Zhang, Y., Jeppesen, E., de Souza, J.G., Wu, H., Shi, K., Qin, B., 2018. How autochthonous dissolved organic matter responds to eutrophication and climate warming: evidence from a cross-continental data analysis and experiments. Earth Sci. Rev. 185, 928–937.